Available online at www.sciencedirect.com
SCIENCE DIRECT®
Proceedings of the Combustion Institute 30 (2005) 701–709
Proceedings of the Combustion Institute
www.elsevier.com/locate/proci

Experimental analysis of local flame extinction in a turbulent jet diffusion flame by high repetition 2-D laser techniques and multi-scalar measurements

J. Hult[a,c,*], U. Meier[b], W. Meier[b], A. Harvey[c], C.F. Kaminski[c]

[a] Department of Combustion Physics, Lund Institute of Technology, P.O. Box 118, SE-22100 Lund, Sweden
[b] DLR, Institut für Verbennungstechnik, Pfaffenwaldring 38-40, D-70569, Stuttgart, Germany
[c] Department of Chemical Engineering, University of Cambridge, Pembroke Street, Cambridge CB2 3RA, UK

Abstract

In this paper, we present a detailed experimental study of turbulence chemistry interactions in the "DLR_B" turbulent jet diffusion flame. The flame operates on mixtures of CH_4, H_2, and N_2 in the fuel stream at $Re = 22{,}800$ and is a target flame within the TNF workshop. Extinction and re-ignition events can be tracked in real time and related to the underlying flow field phenomena and temperature fields. Time resolved measurements of OH radical concentration fields are performed in combination with temperature and velocity field measurements. For this purpose, we combined high repetition rate (33 kHz) PLIF imaging with stereoscopic PIV and double pulse Rayleigh imaging techniques. Comparisons are made with results from multi-scalar Raman/Rayleigh/LIF point measurements that reveal the thermochemical state of the flame. The large deviations from equilibrium observed on resulting OH/temperature joint pdfs could be related to strain rate and Damköhler number variations caused by turbulent flow structures leading to frequent extinctions. The 2D measurement series uniquely reveal the underlying mechanism that can lead to such events. Finally, comparisons are made to strained laminar flame calculations, which are generally found to be in good agreement with the measured data.

Keywords: Laser diagnostics; PLIF; Multi-scalar diagnostics; Non-premixed flame; Turbulence/chemistry interactions

1. Introduction

For the understanding and simulation of turbulent combustion processes, effects of turbulence-chemistry interaction play an important role. When a vortex interacts with a flame front, the straining of the reaction zone can lead to a temperature reduction and a thinning of the flame front. The flame chemistry responds with deviations from equilibrium, and the flame eventually extinguishes if exposed to high strain rates for a sufficiently long time. For laminar flames, measurements of the interaction between the reaction zone and reproducibly generated vortices have revealed details of the underlying mechanisms [1–3]. However, in turbulent flames the situation is more complex, and a detailed characterization needs more sophisticated measuring strategies.

A number of experimental investigations in turbulent jet flames characterized the thermochemical state, e.g., by Raman or Raman/LIF measurements [4–6], or the structures by planar

* Corresponding author. Fax: +44 01223 334796.
E-mail address: jfh36@cheng.cam.ac.uk (J. Hult).

1540-7489/$ - see front matter
doi:10.1016/j.proci.2004.08.069

laser-induced fluorescence (PLIF) of OH or CH, in some cases combined with particle image velocimetry (PIV) [7–13], or combined with Rayleigh scattering [14–16]. These single-pulse measurements yielded information about the instantaneous flame behavior. The temporal development has been studied by point-measurements, e.g., of OH [17], but hardly by two-dimensional (2D) imaging techniques. The unique high-speed imaging facility at the Lund Institute of Technology [18,19] has extended the use of "standard" 2D laser techniques into the time domain. Here, we report on the combination of such techniques to study a turbulent jet flame, to yield insight into the temporal development of turbulent flame structures, and to reveal details of effects of turbulence-chemistry interactions.

In this study, we combined high repetition rate PLIF with either double-pulse Rayleigh or stereoscopic-PIV imaging to record a series of OH images simultaneously with temperature fields or three-component velocity fields. Experiments were performed in a $CH_4/H_2/N_2$ jet diffusion flame previously studied in several laboratories using different techniques [20–23]. The flame is a "target flame" (termed DLR_B Flame) of the International Workshop on Turbulent Non-premixed Flames [24].

Pointwise Raman and Raman/Rayleigh/LIF measurements performed in identical flames at the German Aerospace Center (DLR) and at the Sandia National Laboratories yielded the joint probability density functions of the mole fractions of the major species, OH, and NO, together with the temperature and mixture fraction [20,21]. These measurements shed light on the thermochemical state of the flame and identified finite-rate chemistry effects during flame extinction. The combined results from the 2D time series and the single-point multi-species measurements represent a comprehensive database, which explains the physical and chemical processes in the flame under investigation with emphasis on events of local flame extinction. In this paper, exemplary results from the large amount of experimental data are presented with the focus on extinction phenomena. Besides the demonstration of experimental techniques, the main goal was a detailed analysis of the turbulence-chemistry interactions in this flame.

2. Experiment and data processing

The burner consists of a straight tube ($l = 350$ mm, *i.d.* $= 8$ mm) with a thinned rim at the exit, surrounded by a co-flow nozzle for air. The fuel had a composition of 22.1% CH_4, 33.2% H_2, and 44.7% N_2 and a mean exit velocity of 63.2 m/s ($Re = 22{,}800$), the coflow velocity was 0.3 m/s. The stoichiometric mixture fraction is $f_{\text{stoich.}} = 0.167$, and the adiabatic flame temperature is $T_{\text{ad.}} = 2130$ K. The flame is operated as a free jet without pilot flame and, at $Re = 22{,}800$, the flame is close to blow off with frequent events of localized flame extinction and re-ignition. The flame length, defined as the height where f_{mean} is equal to $f_{\text{stoich.}}$, is about 560 mm. The fuel composition enables the application of Rayleigh thermometry without knowledge of the local gas composition, because the effective Rayleigh scattering cross-section varies only by ±3% over the range of possible mixtures of fuel, air, and exhaust gases [20]. For the PIV measurements, both the fuel and air flows were seeded with $d = 1$ μm titanium dioxide (TiO_2) particles gathered from a fluidized bed seeder (fuel flow) and a cyclone seeder (coflow).

The Lund high-speed imaging facility [18,19] was used to acquire high repetition-rate OH PLIF sequences, consisting of six individual images separated by 30 μs time intervals. The pulse bursts were delivered by 4 double pulsed, frequency doubled Nd:YAG lasers, fired in rapid succession. A frequency doubled dye laser, pumped by six of the Nd:YAG pulses, was used to excite OH via the $Q_1(8)$ transition in the $v'' = 0$, $v' = 1$ band of the $A^2\,\Sigma^+ \leftarrow X^2\Pi$ system (~283 nm, 4 mJ energy per pulse). Laser sheets were measured to be 35 mm across and about 0.3 mm in width in the interaction region. OH fluorescence from the $v'' = 0$, $v' = 0$ and $v'' = 1$, $v' = 1$ bands was detected using a fast framing camera (Imacon 468, DRS Hadland), consisting of 8 ICCDs (8 bit dynamic range, 576×384 pixels). The camera was fitted with an $f = 100$ mm achromatic UV lens (Bernhard Halle, *f*/2) and filtered using a 295 nm high-pass filter (LaserOptik) in combination with a UG 11 filter, to reject scattered laser light. The resolution of the OH PLIF data was around $(0.3\text{ mm})^2$. Signal-to-noise ratios exceeded 15 at all times. The PLIF data were not calibrated to yield absolute OH concentrations, but relative intensities should represent relative OH concentrations to better than 30% [14]. A cell filled with fluorescing dye solution and two quartz plates were used to perform an on-line beam profile measurement to compensate for pulse-to-pulse fluctuations in the dye laser profile [19]. The OH PLIF images were mapped on top of each other using a polynomial coordinate mapping algorithm described in [25]. Source and target mapping co-ordinates were obtained from imaging common targets containing a series of crosshairs in the measurement plane. A similar procedure was used to map the OH images onto the PIV or Rayleigh images. OH images were divided by the recorded laser intensity profiles (where available) on a shot-by-shot basis to compensate for laser beam inhomogeneities.

The PIV measurements were performed with a commercial stereoscopic PIV system (OFS Ltd/

ILA). The laser source was a diode pumped twin Nd:YAG laser system (Quantel, "Twins Ultra") with a pulse energy of 40 mJ at 532 nm. The PIV laser sheets were overlapped with the PLIF sheets in a counterpropagating configuration as shown in Fig. 1. Two frame transfer CCD cameras (PCO Sensicam, 12 bit, 1280×1024 pixels) were mounted at 60° to each other in a Scheimpflug configuration [26] to detect the Mie scattering from the seeded particles. Each camera was fitted with an interference narrow bandpass filter ($\lambda = 532$ nm) to reject flame emission. A separation of 10.3 μs between the PIV pulses was used, with the first pulse fired 5 μs before the 3rd PLIF pulse, and the second pulse fired 5.3 μs after the 3rd PLIF pulse.

The *vidPIV* processing software (ILA, Germany) was used for velocity calculations. After applying an edge detection method to sharpen the image, the data were cross-correlated at successively smaller interrogation areas, with interpolation in between each. After the final cross-correlation, using an interrogation region of 32×32 pixels, which corresponds to 0.5×0.5 mm, and window filtering the data were subjected to median filtering and interpolation. Finally, the two velocity fields thus extracted from the two individual cameras were combined to yield three-component velocity vectors. Errors were less than ±1 m/s in the cold fuel stream and less than ±3 m/s in the hot burned regions.

From the in-plane velocity components, four components of the strain rate tensor could be calculated, the tensor was then transformed to principal coordinates, giving the two principal strain rates. The maximum principal strain rate component corresponds to extensive strain, and the minimum component to compressive strain. Principal strain rates computed from 2D measurement data are only valid in regions where the flow is locally 2D or where the z-axis is already a principal axis [27]. One of the advantages of using stereoscopic PIV is that regions of strong 3D flow character, where the calculated strain rates are invalid, can be directly identified. The main contribution to errors in the calculated strain rate fields comes from errors in the corresponding velocity fields. Following the approach in [27], these were estimated to be $1000\ s^{-1}$ in the cold regions and $3000\ s^{-1}$ in the hot regions.

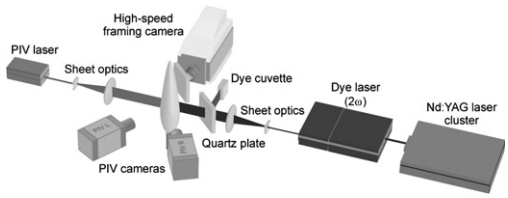

Fig. 1. Experimental set-up used for simultaneous high-speed OH PLIF and stereoscopic PIV measurements.

For the Rayleigh scattering experiments, 2 pulses from the Nd:YAG cluster were frequency doubled to 266 nm (~40 mJ per pulse), formed into a sheet of similar dimensions as used for OH PLIF, and adjusted to coincide with the PLIF measurement plane in the flame. The setup was similar to the one shown in Fig. 1, except that the Rayleigh cameras were arranged at a much smaller angle than the PIV cameras (13°). Optics for PLIF beam profile measurements described above were removed, as they were found to introduce unacceptable amounts of laser scatter on the Rayleigh signal detectors. The Rayleigh images were spaced at $\Delta t = 90$ μs and synchronized with the first and fourth images of each OH PLIF sequence. Two separate gated 12 bit ICCD cameras (Flame Star, LaVision, 384×286 pixels) equipped with $f = 105$ mm UV lenses (Nikon, $f/4.5$) were used for imaging the Rayleigh signal.

The Rayleigh signals in the flame images were divided by an average image recorded in room temperature air at 300 K, to normalize the images with respect to the inhomogeneous intensity distribution across the light sheet. In addition, the room temperature signal S_{room} can provide a reference for calibration of the flame signal S_{flame}, which yields a flame temperature T_{flame} according to $T_{\text{flame}} = T_{\text{room}} S_{\text{room}} / S_{\text{flame}}$, under the assumption of a constant Rayleigh scattering cross-section. This assumption is justified for the fuel compositions reported here [20]. However, since the relatively weak signals in the hot regions were suspected to contain an unknown contribution from scattered light, which could not be measured separately, the Rayleigh signals were normalized using radial temperature profiles measured by Raman scattering at axial distances of $x/D = 5$ and 10, respectively. The Rayleigh images were smoothed (filter width: 5 pixels) before the temperature was calculated, resulting in a resolution of 0.35 mm. SNRs in the burned gases limit the accuracy of temperature data to around 400 K.

The results from Raman/Rayleigh/LIF measurements presented in this paper have been obtained at the Sandia National Laboratories using Raman scattering for the determination of the mole fractions of O_2, N_2, CH_4, H_2, H_2O, and CO_2, and LIF for the quantitative measurement of CO, OH, and NO. Details of the experiment are given in [21].

3. Results

3.1. Velocity field and flame front evolution

Figure 2 shows three examples of OH PLIF sequences obtained from the non-premixed jet flame ($Re = 22{,}800$ flame) described above.

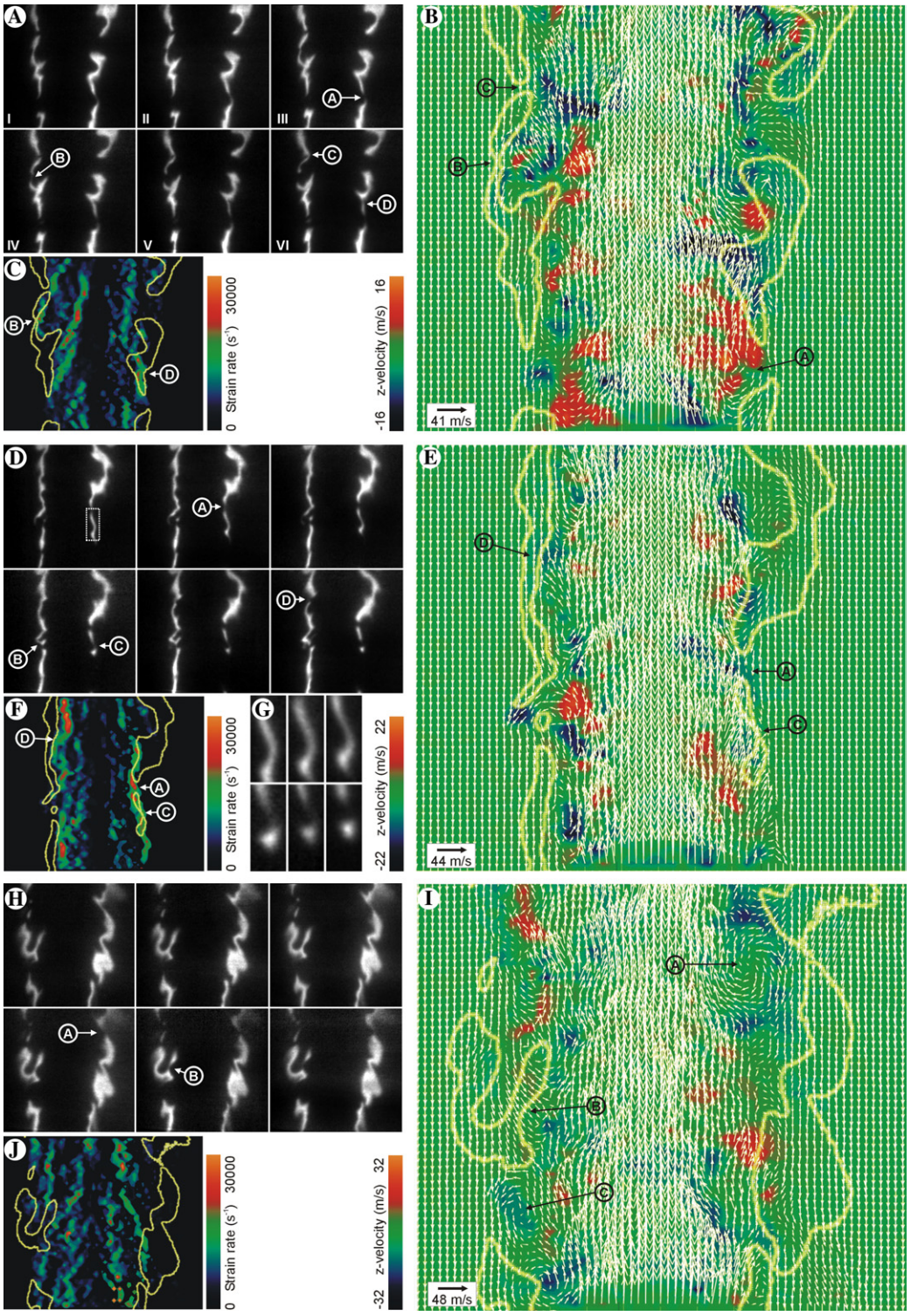

Fig. 2. (A, D, and H) Three examples of OH time sequences. The time difference between individual images is 30 μs, and the image region corresponds to 32×30 mm^2 ((A and D) $x/D = 4.5$–8.25; (H) $x/D = 8$–11.75). (B, E, and I) PIV images recorded corresponding to the 3rd frame in the OH sequences. (C, F, and J) Maximum principal strain rates. (G) Magnified view of the region indicated by rectangle in (D).

For sequence (a) the imaged region corresponds to between 4.5 and 8.25 nozzle diameters in height above the nozzle exit plane (image size: 32×30 mm, time separation between images: 30 μs). Figure 2B shows the PIV measurement, that was synchronously recorded with the 3rd frame of the OH sequence. The mean flow velocity over the measurement region was subtracted from the velocity field to enhance the appearance of flow structures near the flame front. To aid in interpretation of observed phenomena, OH contours from the 3rd PLIF frame are overlaid in white on the velocity plot. The maximum component of the principal strain rate is plotted in Fig. 2C. The maximum principal strain rates are all positive, corresponding to extensive strain. From the images, it is seen that thin flame fronts, corresponding to regions of high OH concentrations, prevail (0.5–3 mm). Najm et al. [28] have shown that disruptions in otherwise continuous OH fronts correlate well with local flame front extinctions. Several such extinct regions are seen in the first frame of Fig. 2A. Apart from the already extinct areas, the occurrence of new extinction events is evident from the OH sequence, indicated by the arrows in the lower right (A) and upper left (B) parts of the PLIF and PIV images. Such events are recognizable only from time sequenced measurements, such as shown. A re-ignition event is also seen to take place (C). A common problem with 2D imaging of such events has been the ambiguity associated with motion into (or out of) the measurement plane. For example, the highlighted events could have been due to convective motion of an already extinct pocket into the measurement plane. That this is not the case in regions (B) and (C) is seen from the stereoscopic PIV data: out-of-plane velocity components, represented by the background color scale, are close to zero. At the location of (A), however, there is a strong flow component perpendicular to the measurement plane. This demonstrates that the interpretation of extinction events from 2D measurement techniques has to be conducted with caution [19,11].

In most regions defined by the OH contours, the flow is seen to be laminarized by the higher viscosity of the burned gases (the kinematic viscosity changes approximately by a factor of 15 from unburned to burned gases). In contrast, on the fuel-rich side of the flame front and also in regions of extinction, strong vortical motion is still evident.

The information afforded by these combined measurements allows an interpretation of the possible physical phenomena taking place in these turbulence/chemistry interactions. For example, in region (A), Fig. 2A, the extinction seems to be caused by a large fuel vortex breaking through the OH layer, which is weak but still intact in the first two frames of the PLIF sequence. Furthermore, the flame lip just above the resulting OH gap is seen to correspond to a region of very high extensive strain, above 15,000 s^{-1} (see region (D), Fig. 2A). The OH lip is thinning in time and becomes less intense at the end of the sequence, presumably due to increased heat losses associated with increasing scalar dissipation rates. At extinction location (B), strain rates are high on the fuel side of the OH layer, and there is a strong velocity component directed towards the flame front. It is interesting to note that regions of highest strain rates and vorticity (data not shown) do not, in general, correlate with the locations of the OH front. This phenomenon has been previously observed by Rehm and Clemens [27] who found a good correlation between flame front and vorticity field locations in low *Re*-number flames, and weaker correlations for higher *Re*-number flows. The reason for this is that in laminar like flows the jet velocity is mostly dissipated within the reaction zone, leading to locally high strain (and thus vorticity). This laminarization effect becomes less important for very high *Re*-number flames. Narrow regions of high strain rates, above 10,000 s^{-1}, appear in Figs. 2C and F, with peak values exceeding 20,000 s^{-1}, which is in agreement with peak values previously reported in similar non-premixed turbulent flames [11]. Outside these localized regions, however, strain rates are generally much lower. Laminar flames subjected to continuous strain are observed to extinguish at much lower strain rates than the instantaneous peak values observed here. In the present case, the flame may be subjected to such high strains for only very short times.

The sequence in Fig. 2D shows extinction events (A, C, and D) of a different nature to the one observed in sequence (a) and also a re-ignition event (B). Flow conditions are the same as for the previous sequence, however here extinctions are caused by high local strain fields rather than fuel vortices. Strain rates are seen to be very high, above 15,000 s^{-1}, within the extinguishing regions, Fig. 2F (A, C, and D), whereas corresponding flow field data indicate no strong vortical structures near these locations. The OH braids are laminar-like, but are thinning and stretching in regions of high strain, this thinning is clearly seen in Fig. 2G, which shows a magnified view of event (C) in Fig. 2D. The increased thinning of the strained flame front and associated increase in scalar dissipation rates cause the flame to extinguish in time. All extinction events observed seem to occur on a 60–120 μs time scale, during which the OH front changes from intact to completely broken.

Figure 2H corresponds to a sequence higher up in the flame at $x/D = 8$–11.75. Here, the OH field appears strongly corrugated, and much larger vortices have developed in the fuel flow. Most of the extinction events seem to be associated with the

movement of large flow structures near the OH fronts, see Fig. 2I (A and B). From all the image sequences shown so far, it is seen that where the reaction front is intact it acts as a shield to prevent fuel and hot products from the fuel rich side to escape to the outside of the flame. In regions where extinction has occurred, this is not the case: e.g., the large vortex seen in Fig. 2I (arrow C) shows how fuel and products can escape to the outside and mix with air to produce partially premixed regions that could later ignite. This supposition is supported by the Rayleigh-OH data discussed below.

3.2. Temperature field and flame front evolution

Figure 3 shows two examples of simultaneous flame front and temperature measurements obtained by combining the OH PLIF measurement sequence with two Rayleigh measurements. The Rayleigh images were concurrent with the 1st and 4th frames of the OH sequence. The temperature data typically have a diffusive appearance towards the jet center line (fuel rich regions) due to turbulent mixing, consistent with the evidence from the OH-PIV sequences shown in Fig. 2. Despite high temperatures prevailing quite a long way into the fuel stream, away from the flame front, the OH disappears rapidly. This is supported by laminar flame calculations, which show that at high strain rates OH is present at $T \geqslant 800$–900 K on the lean side, but only above ≈1700 K on the rich side (see Fig. 4 and corresponding discussion in Section 3.3).

In sequence (A), an extinction event (A) is seen to be accompanied by a large temperature drop from the first to the second Rayleigh image in the sequence, two more extinction events (D) being evident in sequence (B). In sequence (B), an example of reignition is also seen (E), where the reappearance of high OH concentrations at

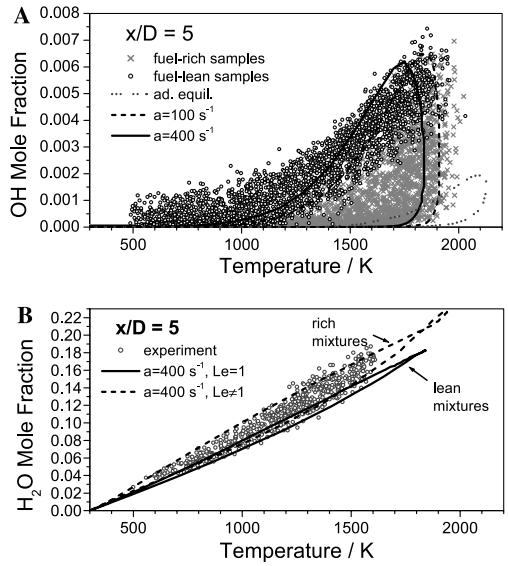

Fig. 4. (A) Correlation between OH and T at $x/D = 5$. The different symbols distinguish between samples with $f < f_{\text{stoich.}}$ and $f > f_{\text{stoich.}}$. Calculations were performed for constant Lewis number $Le = 1$. (B) Correlation between H_2O and T showing only samples with large deviations from equilibrium temperature. The curves show calculations with and without Lewis number effects ($Le \neq 1$, $Le = 1$) [21].

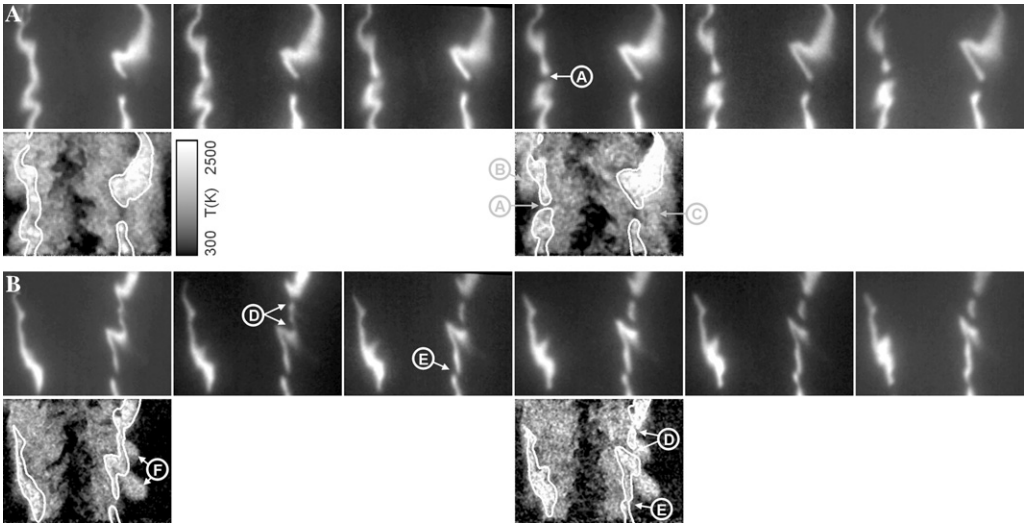

Fig. 3. Example of OH time sequences and Rayleigh temperature sequences. The time difference between individual images is 30 μs, and the image region corresponds to a height of $x/D = 5$–7.5. The corresponding Rayleigh images were simultaneously recorded with the 1st and 4th frames in the OH sequences.

a break in the flame front is seen to be accompanied by a local temperature rise in the Rayleigh data.

In both sequences, pockets of hot gas are also observed outside the flame front (B, C, and F). As long as the flame front is connected, fuel-rich mixtures prevail on the inside of the flame front and fuel-lean mixtures outside. If the flame front is interrupted, the high-viscosity layer is no longer present to form a barrier for turbulent eddies and fuel-rich gas with intermediate temperature and low OH concentrations can "escape" through the hole in the reaction zone. This is also supported by the PIV/PLIF data, see, for example, Fig. 2I, event (C), and the corresponding discussion above. The mixing of this gas with air can lead to partially premixed compositions that may subsequently lead to reignition. Such phenomena may be behind the reignition events found in both Figs. 2A and D.

3.3. Thermochemical state

The thermochemical state of the flame changes with downstream position from "significant non-equilibrium effects" in the start region to "near equilibrium" at the flame tip [21]. For the region $x/D \leqslant 10$ which is considered in this paper, the majority of the single-shot results exhibit a thermochemical state that is in accordance with strained laminar flame calculations with strain rates of the order of $a = 100$–$400\ \mathrm{s}^{-1}$. However, a few percent of the samples exhibit pronounced deviations from the calculations and have to be interpreted as the result from local flame extinction events (see Fig. 9 in [21]). The correlation between OH and T at $x/D = 5$ is shown in Fig. 4A. Each symbol represents the result of a single-shot measurement performed at various radial locations, and samples from fuel-lean and fuel-rich mixtures are distinguished by different symbols. The curves show adiabatic equilibrium and the results from strained laminar flame calculations with $a = 100$ and $400\ \mathrm{s}^{-1}$[29,30]. The following observations are important to note: (1) The measured OH mole fractions exceed the adiabatic equilibrium value by up to a factor of about 3 and are very well reproduced by the strained laminar calculations. (2) The experimental and calculated results clearly demonstrate the different dependences of OH concentration on temperature in fuel-lean and fuel-rich mixtures. At a strain rate of $a = 400\ \mathrm{s}^{-1}$, noticeable OH concentrations already appear at 800–900 K on the lean side, but only at $T > 1700$ K on the rich side. This behavior changes with the strain rate. These findings are clearly supported by the observations discussed in Section 3.2 and the corresponding Rayleigh/OH data in Fig. 3. (3) The scatter in the experimental results is partly due to measuring precision (±10% for OH) and also influenced by spatial averaging effects (at $x/D = 5$, spatial gradients can be large in a measuring volume of 0.8 mm). However, the major contribution to the scatter stems from the flame itself and reflects the effects of turbulence/chemistry interactions so frequently observed in the planar imaging data.

Statistics were performed on samples with large deviations from equilibrium, which were most probably involved in local flame extinction events. The criterion for their selection was a temperature drop of $\Delta T \geqslant 300$ K compared to the laminar flame calculation with $a = 100\ \mathrm{s}^{-1}$. These samples span a temperature range from 500 to 1600 K and are characterized by the coexistence of fuel and air. The correlation between H_2O mole fraction and T, displayed in Fig. 4B, exhibits only little scatter and is in reasonable agreement with strained laminar flame calculations indicating partial equilibrium between these quantities. The OH mole fractions of these samples do not exhibit a clear correlation with T, f, or any other quantity. About 50% of the samples contain almost no OH consistent with the large number of extinction events observed on the PLIF sequences.

4. Conclusions

A detailed study of turbulence/chemistry interaction events in a fully turbulent non-premixed jet flame has been presented. Sequences of high-repetition rate OH PLIF were simultaneously performed either with stereoscopic PIV imaging or with double-pulse Rayleigh temperature imaging. The temporal evolution of extinction events could thus be correlated to the behavior of temperature and velocity fields.

Individual extinction events could be correlated to local strain rate fields and vortical flow structures. Ambiguities associated with out-of-plane motion, affecting previously reported 2D measurements, were avoided by the use of stereoscopic PIV. Instantaneous values of the strain rates were often orders of magnitude above extinction limits for laminar flames.

Laminarization in the reaction zone provides an effective shield preventing fuel vortices from penetrating through the flame front. However, vortical structures may escape where the flame is extinct, which could lead to partially premixed regions at an intermediate temperature that could subsequently ignite. The Raman/Rayleigh/LIF measurements revealed pronounced deviations from equilibrium composition and temperature, and a large scatter in OH concentrations in the start region of the flame, where strong variations in local strain rates and Damköhler numbers are present, which frequently led to localized extinction events.

Acknowledgments

We thank Prof. M Aldén for general support and Prof. M. Mackley for loan of experimental equipment. We also thank R. Barlow for his contributions to the Raman/Rayleigh/LIF measurements, and Prof. J.-Y. Chen for provision of strained laminar flame calculations. This work was supported by the Swedish Research Council, the Swedish Energy Administration, and an EPSRC platform Grant: GR/R98679/01. U.M. and C.F.K. acknowledge support by the Lund Laser Centre as part of the European Large Scale Facility Programme (EC contract number ERB-FMGECT-950020). J.H. has been supported by a Marie Curie Fellowship of the European Community Human Potential programme, under contract number HPMF-CT-2002-01574.

References

[1] Q.-V. Nguyen, P.H. Paul, *Proc. Combust. Inst.* 26 (1996) 357–364.
[2] C.M. Vagelopoulos, J.H. Frank, *Proc. Combust. Inst.* 29 (2002) 1721–1728.
[3] P.-H. Renard, J.C. Rolon, D. Thévenin, S. Candel, *Combust. Flame* 117 (1999) 189–205.
[4] A.R. Masri, R.W. Dibble, R.S. Barlow, *Prog. Energy Combust. Sci.* 22 (1996) 307–362.
[5] A. Neuber, G. Krieger, M. Tacke, E. Hassel, J. Janicka, *Combust. Flame* 113 (1998) 198–211.
[6] R.S. Barlow, C.D. Carter, R.W. Pitz, in: K. Kohse-Höinghaus, J. Jeffries (Eds.), *Applied Combustion Diagnostics*. Taylor & Francis, New York, 2002, p. 384.
[7] J.E. Rehm, N.T. Clemens, *Proc. Combust. Inst.* 27 (1998) 1113–1120.
[8] J.H. Frank, P.A.M. Kalt, R.W. Bilger, *Combust. Flame* 116 (1999) 220–232.
[9] J.E. Rehm, N.T. Clemens, *Combust. Flame* 116 (1999) 615–626.
[10] D. Han, M.G. Mungal, *Proc. Combust. Inst.* 28 (2000) 261–267.
[11] J.M. Donbar, J.F. Driscoll, C.D. Carter, *Combust. Flame* 125 (2001) 1239–1257.
[12] K.A. Watson, K.M. Lyons, C.D. Carter, J.M. Donbar, *Proc. Combust. Inst.* 29 (2002) 1905–1912.
[13] P.S. Kothnur, M.S. Tsurikov, N.T. Clemens, J.M. Donbar, C.D. Carter, *Proc. Combust. Inst.* 29 (2002) 1921–1927.
[14] J. Kelman, A.R. Masri, *Appl. Opt.* 36 (1997) 3506–3514.
[15] S. Böckle, J. Kazenwadel, T. Kunzelmann, D.-I. Shin, C. Schulz, J. Wolfrum, *Proc. Combust. Inst.* 28 (2000) 279–286.
[16] K.A. Watson, K.M. Lyons, J.M. Donbar, *Combust. Flame* 123 (2000) 252–265.
[17] M.W. Renfro, G.B. King, N.M. Laurendeau, *Appl. Opt.* 38 (1999) 4596–4608.
[18] C.F. Kaminski, J. Hult, M. Aldén, *Appl. Phys. B* 68 (1999) 757–760.
[19] J. Hult, Ph.D. Thesis, Lund Institute of Technology, Lund, Sweden, 2002.
[20] V. Bergmann, W. Meier, D. Wolff, W. Stricker, *Appl. Phys. B* 66 (1998) 489–502.
[21] W. Meier, R.S. Barlow, Y.-L. Chen, J.-Y. Chen, *Combust. Flame* 123 (2000) 326–343.
[22] M.W. Renfro, W.A. Guttenfelder, G.B. King, N.M. Laurendeau, *Combust. Flame* 123 (2000) 389–401.
[23] Y. Zheng, Y.R. Sivathanu, J.P. Gore, *Proc. Combust. Inst.* 29 (2002) 1957–1963.
[24] Available from: <http://www.ca.sandia.gov/TNF>.
[25] M. Sonka, V. Hlavac, R. Boyle, *Image Processing, Analysis and Machine Vision.* Chapman & Hall, London, UK, 1993.
[26] M. Raffel, C. Willert, J. Kompenhans, *Particle Image Velocimetry*. Springer, ISBN 3-540-63683-8, 1998.
[27] J.E. Rehm, N.T. Clemens, American Institute of Aeronautics and Astronatics, Reston, VA., Paper No. AIAA-99-0676, 1999.
[28] H.N. Najm, P.H. Paul, C.J. Mueller, P.S. Wyckoff, *Combust. Flame.* 113 (1998) 312–332.
[29] J.-Y. Chen, *Private communication*, 1999.
[30] J.H. Miller, R.J. Kee, M.D. Smooke, J.F. Grcar, *Paper WSS/CI 84-10,* Western State Section of the Combust. Inst., Spring Meeting, 1984.

Comments

Graham Nathan, University of Adelaide, Australia. Please comment on the accuracy of your strain rate measurements, specifically regarding:

1. The effect of thermophoresis and whether you were able to quantify this from your temperature measurements.
2. The limitation of light sheet thickness on spatial resolution.

Reply. Thermophoresis affects the accuracy of the strain component across the flame front where the temperature gradients are highest. Based on the thermophoretic diffusivity off 1 μm TiO_2 particles, the kinematic viscosity, and maximum possible temperature gradients in the present flame we estimate the error to a maximum of 6 percent on the mean strain rate values reported here. In principle the Rayleigh data could be used to estimate this effect, however, the moderate signal to noise ratios obtained would not permit us to obtain accurate gradient information and thermophoretic velocities would likely be underestimated in such an approach.

The laser sheet thickness and size of interrogation regions limit the maximal strain rates that can be measured by PIV. Based on peak gas flow velocities present in our flame the maximum strain rates we report in our paper are not limited by this effect.

•

Mohy S. Mansour, The American University in Cairo, Egypt. How accurately can you identify extinction

events considering 3-D effects in your measurements? Considering OH as a marker for the reaction zone is not in all cases true due to its longer lifetime. Using formaldehyde is more accurate. Can you comment on this?

Reply. In principle, out of plane velocity components could lead to artifacts that appear like extinction events on a 2-D planar light sheet measurement, for example convection of an already extinct flame region into the measurement plane. The simultaneously performed 3-D PIV measurement allowed us to identify whether significant out of plane motion occurred in the proximity of potential local extinction events and to discard such data from analysis.

OH is an excellent marker of the reaction zone over the spatial domains imaged in the present work. Measurements where performed close to the nozzle exit where the flow is laminarized in the reaction zones due to the heat release and increase of viscosity. Here, the OH layers are thin and restricted to the reaction zones. The validity of OH as a reaction zone marker in these regions has been confirmed in a previous study of this flame (Ref. [20] in paper) where measurements of the CH layers yielded the same structures. Further downstream in the flame the turbulence is fully developed and the long lifetimes of OH can indeed lead to convective transport of OH away from the flame front and here this approach would not be valid. Formaldehyde, CH_2O was not used because of its lower concentration in the flame (approx. a factor of 50) and its strong dependence of the Boltzmann fraction on temperature.

●

Heinz Pitsch, Stanford University, USA. In a recent study by Sripakagarn, Kosaly, and Pitsch, to appear in Journal of Fluid Mechanics, we investigated extinction and re-ignition in non-premixed turbulent combustion using direct numerical simulations. We found essentially two different scenarios for re-ignition. The first is governed by edge flame propagation, the second by turbulent mixing bringing burning and non-burning sheets together, which leads to a merging of these regions and thereby re-ignition. In your experiments, it seems that you mainly find the edge flame re-ignition mode. Do you see the turbulent mixing mode in your experiments? Especially further downstream, this might become more important. Can the relative importance of the two be quantified?

Reply. It does indeed seem as if most re-ignition events in our flame are governed by edge flame propagation. From our data we do not see evidence that re-ignition via the turbulent mixing mode takes place in the upstream regions of the flame that we study in this paper. We have not studied re-ignition in downstream regions of the flame where a different approach has to be adopted to image the reaction zone layer (e.g. CH imaging, see reply to question by M.S. Mansour).

●

Alesandro Gomez, Yale University, USA. 1. The onset of local extinction and the analysis of edge flame propagation has been addressed in much simpler environments such as laminar flames perturbed by vortices. I wonder if you have tried to analyze your data (e.g. PIV and OH fluorescence) to infer the behavior of your extinction holes from the vantage point of edge flame propagation.

2. You discuss the occurrence of extinction at relatively low strain rate. Since the Damköhler number controls extinction, one can trigger it either by lowering the fluid time (high strain rate) or increasing the chemical time. Is your observation due to increasing the chemical time, via, for example, dilution effects?

Reply. 1. See reply to the Pitsch comment

2. One possible explanation for the mechanism leading to extinction at low strain rates may be that air seeps through holes in the flame front and meets the flame on the fuel rich side, thus starving the flame of combustible mixture. This theory seems to be supported by recent DNS work (J. Chen, private communication) but further experimental work needs to be carried out to verify this hypothesis. One possibility would be to track the airflow using a tracer species such as acetone.